OPEN ACCESS

ARTICLE

Journal homepage: www.the-innovation.org/energy-use

Energy Use

Energy Use 1 (2025):100004

Contents lists available at INNOVATION PRESS

Corrosion-Resistant Amino Acid-Based Deep Eutectic Solvents toward Liquid Desiccant Air Conditioning Systems

Zhiyong Li,[1] Jielin Luo,[1,2,*] and Hongxing Yang[1,*]

*Correspondence: luojielin@mail.sysu.edu.cn (J. L.); hong-xing.yang@polyu.edu.hk (H. Y.)

Received: August 21, 2025; Accepted: September 11, 2025; Published Online: September 25, 2025; https://doi.org/10.59717/ipj.energy-use.2025.100004

GRAPHICAL ABSTRACT

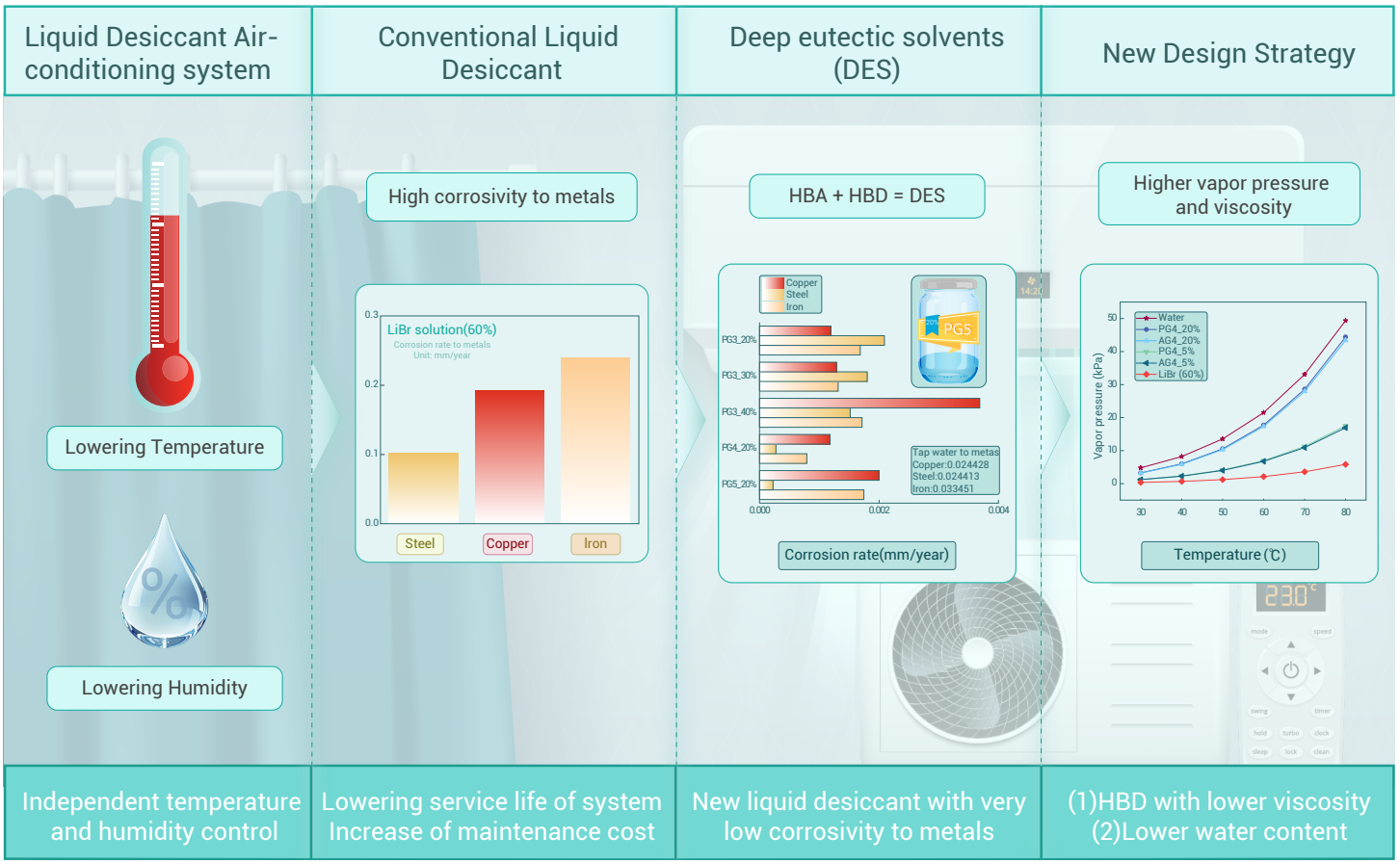

PUBLIC SUMMARY

- Deep eutectic solvents (DESs) offer low-corrosion alternatives to traditional liquid desiccants.
- L-Arginine as HBA enhances robust hydrogen bond networks; HBD ratio and water content influence properties.
- Density, viscosity, and surface tension decrease with higher HBD ratio and water content, except for PG series.
- Vapor pressure drops with increasing HBD ratio but rises with higher water content in DESs.
- DESs show significantly lower corrosion rates than LiBr, with rates as low as 0.001 mm/year on metals.

ARTICLE

OPEN ACCESS

Journal homepage: www.the-innovation.org/energy-use

Energy Use

Energy Use 1 (2025):100004

Contents lists available at INNOVATION PRESS

Corrosion-Resistant Amino Acid-Based Deep Eutectic Solvents toward Liquid Desiccant Air Conditioning Systems

Zhiyong Li,[1] Jielin Luo,[1,2,*] and Hongxing Yang[1,*]

[1]Renewable Energy Research Group, Department of Building Environment and Energy Engineering, The Hong Kong Polytechnic University, Hong Kong SAR, China

[2]School of Advanced Energy, Sun Yat-Sen University, Shenzhen 510275, China

*Correspondence: luojielin@mail.sysu.edu.cn (J. L.); hong-xing.yang@polyu.edu.hk (H. Y.)

Received: August 21, 2025; Accepted: September 11, 2025; Published Online: September 25, 2025; https://doi.org/10.59717/ipj.energy-use.2025.100004

Citation: Li Z., Luo J. and Yang H. (2025). Corrosion-Resistant Amino Acid-Based Deep Eutectic Solvents toward Liquid Desiccant Air Conditioning Systems. *Energy Use* **1**:100004.

Liquid desiccant air-conditioning systems (LDAS) represent a promising energy-efficient technology with considerable potential for reducing overall energy consumption. However, conventional liquid desiccants are hindered by their pronounced corrosivity toward metallic components, which compromises system durability and increases maintenance costs. To address this limitation, the present study explores deep eutectic solvents (DESs) as novel, low-corrosion alternatives for use as liquid desiccants. A comprehensive investigation was conducted to elucidate the effects of hydrogen bond acceptor (HBA) type, water content, and hydrogen bond donor (HBD) ratio on the physicochemical properties of DESs, utilizing both experimental and theoretical approaches. The findings indicate that L-Arginine serves as a particularly effective HBA, promoting the formation of robust hydrogen bond networks within the DES matrix. In general, density, viscosity, and surface tension decreased with increasing HBD ratio and water content, although the surface tension of the Proline-Glycerol (PG) series exhibited an exception to this trend. Concerning vapor pressure, DESs demonstrated a reduction as the HBD ratio increased, but an elevation with higher water content. Importantly, the corrosion rates of the DESs evaluated in this study were significantly lower than those of lithium bromide (LiBr) solution, with values as low as 0.001 mm/year observed on metallic substrates.

INTRODUCTION

In the hot and humid regions, conventional air-conditioning systems account for over 50% of total energy consumption in the building sector.[1] To achieve energy conservation and emission reduction goals, liquid desiccant air-conditioning systems (LDAS) have been proposed as alternatives to conventional vapor compression air-conditioning systems (VCAS), which exhibit high energy consumption. VCAS suffers from two primary drawbacks: the thermodynamically inefficient offsetting of simultaneous heating and cooling loads during fresh air handling. And condensation-induced humidity that promotes microbial growth, thereby compromising indoor environmental health.[2] In contrast, LDAS enables independent temperature and humidity control of fresh air, positioning it as a promising VCAS alternative.[3] However, while common liquid desiccants such as lithium chloride (LiCl) solution,[4] lithium bromide (LiBr) solution,[5] and calcium chloride ($CaCl_2$)[6] solutions demonstrate pronounced dehumidification capabilities, their significant corrosivity toward metallic components remains a critical concern.[7,8] Corrosion induced by these halide-based desiccants not only diminishes LDAS service life but also substantially escalates design and maintenance costs.[9] Consequently, research strategies have focused on incorporating corrosion inhibitors into traditional desiccants or developing novel liquid desiccants exhibiting minimal corrosion rates. Promising low-corrosivity candidates include weak-acid halide solutions, ionic liquids (ILs), and deep eutectic solvents (DESs).[10,11]

To enhance the dehumidification capacity of liquid desiccants, a reduction in their vapor pressure is essential. This creates a greater driving force for mass transfer by increasing the vapor pressure differential between the desiccant and the water vapor in the air stream undergoing treatment. Halide solutions, including LiCl, LiBr, and $CaCl_2$, constitute some of the earliest proposed liquid desiccants primarily owing to their inherently low vapor pressure.[11] Extensive research, encompassing both experimental measurements and empirical correlations, has characterized the effects of concentration and temperature on the vapor pressure of these halide solutions.[12-14] Subsequent efforts to further augment hygroscopic performance have focused on incorporating additives into halide solutions. Okada et al.[15] experimentally demonstrated that activated carbon significantly enhanced the water vapor adsorption capacity of $CaCl_2$ solutions, achieving values up to 0.52 g/g. Similarly, Ye et al.[16] and Wang et al.[17] experimentally illustrated that activated carbon fibre cloth and fibre felts also improve the dehumidification performance of $CaCl_2$ solutions. However, the high crystallization tendency of $CaCl_2$ solutions limits their direct application in LDAS. Therefore, Yao et al.[18] developed an optimized theoretical vapor pressure model for LiCl-$CaCl_2$ solutions based on experimental data. In parallel, Kol et al.[19] reported that integrating carbon nanotubes into LiCl solutions represents a significant enhancement for plate falling-film dehumidifiers. Furthermore, Tsai et al.[20] investigated the impact of adding triethylene glycol or propylene glycol to LiCl or LiBr solutions on key properties, including vapor pressure, density, and viscosity. Their results confirmed a decrease in the vapor pressure following glycol addition. Complementing this work, Krolikowska et al.[21] conducted an experimental study on the effects of ethylene glycol, diethylene glycol, triethylene glycol, and glycerol as additives on the vapor pressure, density, and dynamic viscosity of LiBr solutions.

A well-established inverse relationship exists between the concentration of halide solutions and their vapor pressure, thereby enhancing liquid desiccant dehumidification efficiency. This benefit, however, is counteracted by a concentration-dependent increase in corrosion rates towards copper and steel components, as documented for LiBr solutions.[22,23] Mitigation strategies have focused on incorporating corrosion inhibitors into these desiccants. Li et al.[24] demonstrated that adding an organophosphonate–molybdate inhibitor to LiBr solution reduced the corrosion rate of steel to 0.025 mm/year at 240 °C. Subsequently, Galvez et al.[25] experimentally confirmed that adding $CaCl_2$ or $LiNO_3$ to LiBr solution effectively lowers its corrosion current on carbon steel. Park et al.[26] evaluated the efficacy of various inhibitors—sodium nitrite, sodium hexametaphosphate, trimethylamine,

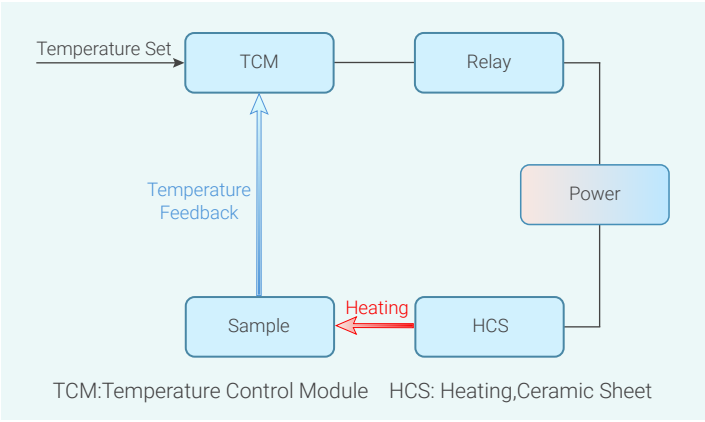

Figure 1. Temperature control system.

sugar, and urea—on mitigating corrosion in $CaCl_2$ solution, identifying sugar as the most effective. Corrosion severity also escalates with concentration in LiCl solutions exposed to carbon steel.[27] Wen et al.[28] achieved a 96.7% reduction in the corrosion rate of hydroxyethyl urea-mixed LiCl solution on stainless steel, as measured electrochemically.

Concurrently, less corrosive and non-volatile alternatives, particularly weak organic acid solutions like potassium formate (HCOOK) and potassium acetate (CH_3COOK), have garnered increased interest for LDAS applications.[29] Wen et al.[30] provided a comprehensive experimental dataset on the thermophysical properties of KCOOH (potassium formate) in 2019. Further validating their potential, Wen et al.[31] demonstrated experimentally in 2020 that a 71% HCOOK solution exhibited a lower corrosion rate on stainless steel compared to a 35% LiCl solution. Subsequent comparative analysis by Wen et al.[32] revealed that a 70.3% HCOOK solution achieved slightly higher absolute moisture removal than a 35% LiCl solution within an LDAS. Corrosion testing by Rippy et al.[33] established that CH_3COOK (potassium acetate) solutions induce corrosion rates on copper and aluminium alloy three orders of magnitude lower than those caused by chloride salt solutions. Nevertheless, the inherently weak moisture absorption capacity of weak organic acid solutions remains a significant bottleneck hindering their broader application.[34]

Ionic liquids (ILs) represent a promising candidate substitute for conventional liquid desiccants, offering potential advantages in dehumidification performance coupled with reduced corrosivity towards metals.[35] Initial investigations into their hygroscopic properties include the experimental characterization of water absorption characteristics for six ILs by Spiess et al.,[36] with quaternary ammonium-based ILs demonstrating particularly low corrosion rates on steel, copper, aluminium, and stainless steel.[37] Comparative performance analysis by Luo et al.[38] revealed that an 81.7% [Dmim][OAc] solution achieved a dehumidification rate comparable to 40.9% LiCl and 45.0% LiBr solutions. Focusing on cost-effectiveness and performance optimization, Qu et al.[39] systematically evaluated 13 different ILs, identifying [EMIM][OAc] as the optimal candidate and providing comprehensive data on its thermophysical properties. However, Wang et al.[40] experimentally demonstrated that the regeneration efficiency of [EMIM][OAc] was lower than its dehumidification efficiency, attributable to its requirement for higher regeneration temperatures. Watanabe et al.[41] further analysed the dehumidification limits and efficiencies of 16 ILs, reporting that tributyl(methyl)phosphonium dimethyl phosphate ($[P_{4441}][DMPO_4]$) exhibited the highest dehumidification limit alongside low metallic corrosion rates.

Significant contributions by Cao et al. include the development of a novel imidazole-based IL possessing exceptionally low vapor pressure, rendering it suitable for deep dehumidification processes.[42] Complementing this, they designed a specialized bubble column dehumidifier for IL operation, demonstrating enhanced efficiency for deep dehumidification,[43] and established a comprehensive mathematical model to analyse the effects of column height, air velocity, and air/solution temperatures on outlet air humidity ratio.[44] Subsequently, they evaluated the efficiency of a falling film dehumidifier utilizing this novel IL (achieving vapor pressures as low as 0.05 kPa) based on a finite difference-based heat and mass transfer model. Their theoretical results indicated that a 90% IL solution yielded a higher moisture removal rate than a 60% LiBr solution.[45] Nevertheless, the practical implementation of ILs faces challenges, including volatility, higher viscosity, and substantially greater cost compared to traditional saline solutions.[10]

Deep eutectic solvents (DESs) are regarded as a promising candidate substitute for conventional saline salt solutions due to their advantageous combination of non-corrosiveness, hygroscopicity, and biodegradability[46] Initial experimental investigations by Oladosu et al.[47] evaluated the dehumidification and thermal regeneration performance of 11 binary DESs within an air-conditioning system, achieving a dehumidification mass flux of 4.61×10^{-2} g/(m^2·s). Subsequent innovations by the same group developed a 3D-printed electrodialysis cell to enhance DES regeneration performance, demonstrating that an applied magnetic field further increased regeneration efficiency.[48, 49] Beyond performance metrics, Luo et al.[50] proposed a comprehensive energy, exergy, exergoeconomic, and enviroeconomic (4E) assessment model to evaluate the application potential of DESs in LDAS. This analysis revealed a substantial 52.36% reduction in CO_2 emissions compared to traditional halide solution desiccants. Further enhancing system viability, Zhang et al.[51] introduced a solar-assisted LDAS utilizing DES alongside LiCl solution as desiccants, thereby improving energy efficiency and expanding applicability. Notably, the system COP with DES was marginally higher than that achieved with LiCl solution. Consequently, the relatively high viscosity of DESs represents a primary limitation for their practical implementation in LDAS.[11]

In summary, the high corrosivity of conventional halide solution desiccants significantly compromises the longevity and maintenance costs of LDAS. Furthermore, the inherently limited moisture absorption capacity of weak acid salt solutions and the prohibitive cost of Ionic Liquids (ILs) constrain their commercial viability. This work addresses these limitations by presenting a novel Deep Eutectic Solvent (DES) formulated using amino acids as the Hydrogen Bond Acceptor (HBA). A comprehensive characterization of its physicochemical properties was conducted through integrated experimental and theoretical methodologies. The influence of water content, HBA type, and Hydrogen Bond Donor (HBD) ratio on key thermophysical properties was systematically analysed. Furthermore, a strategic DES design approach was proposed to achieve the concurrent reduction of viscosity and vapor pressure. Critically, the corrosion rates of this DES on copper, iron, and steel substrates were quantified and benchmarked against those of LiBr solution, demonstrating significantly lower corrosion.

MATERIALS AND METHODS

Preparation of DESs

Deep eutectic solvents (DESs) were synthesized using a constant-temperature stirring method. Hydrogen bond acceptors (HBAs) – specifically L-Arginine (HBA_1) and L-Proline (HBA_2) (Shanghai McLean Biochemical Technology Co., Ltd.) – were combined with hydrogen bond donors (HBDs) – Glycerol (HBD_1) and deionized water (HBD_2) (Shanghai Aladdin Bio-Chem Technology Co., Ltd.) – at predetermined molar ratios (see Table S1). The components were mixed in a beaker and homogenized using a constant-temperature stirrer (Model HH-SA, Changzhou Runhua Equipment Appliance Co., Ltd.) maintained at 80 °C with an agitation speed of 600 rpm for 2 hours. Following synthesis, the resulting DES mixtures were allowed to equilibrate at ambient conditions for 12 hours to ensure phase stability; only optically homogeneous, precipitate-free samples proceeded to thermal property characterization. As illustrated in Figure S1, the Arginine-Glycerol (AG) series exhibited a characteristic light-yellow coloration, while the Proline-Glycerol (PG) series predominantly appeared as transparent white liquids.

Physicochemical Experiment

Thermal properties. The thermophysical properties of the synthesized DES samples—specifically density, viscosity, and surface tension—were characterized using the following calibrated instruments: Density: MDJ-300Y densitometer (Shanghai Yueping Scientific Instrument Co., Ltd.; accuracy: ±0.001 g/cm^3). Viscosity: NDJ-5S rotational viscometer (Shanghai Nirun Intelligent Technology Co., Ltd.; accuracy range: ±0.01–0.1 cp). Surface tension: JBT07B automatic tensiometer (Shanghai Pingxuan Scientific Instrument Co., Ltd.; accuracy: ±0.00001 mN/m). To ensure isothermal measurement conditions across varying temperatures, a custom tempera-

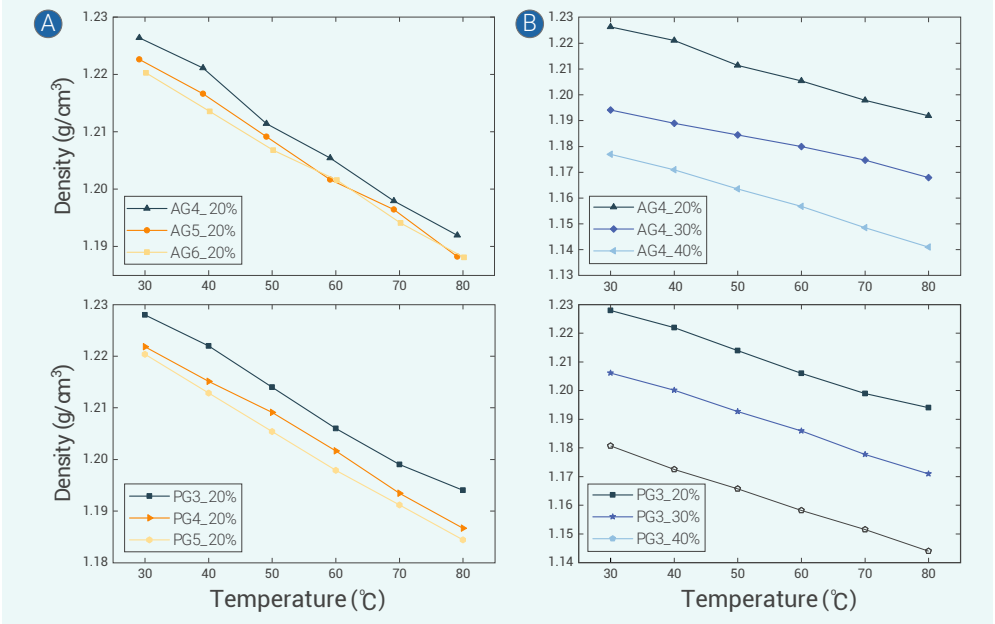

Figure 2. Densities of DESs

ture control system was implemented (schematic shown in Figure 1). This system comprised: YUDIAN AI-208 PID temperature controller (±0.01 °C), G3NA-D210B solid-state relay (OMRON), UTP1310 DC power supply (320 W max; MCH Instruments), Ceramic heating elements (80 W max per unit), K-type thermocouple for closed-loop feedback.

Corrosion rate. The significant corrosivity of conventional liquid desiccants toward metallic components detrimentally impacts the service lifetime of heat exchangers in Liquid Desiccant Air-Conditioning (LDAC) systems. Consequently, quantifying the corrosion rate of Deep Eutectic Solvents (DESs) serves as a critical evaluation metric for comparative assessment against traditional desiccants. Electrochemical corrosion measurements were performed using a standard three-electrode cell configuration, comprising: A metal coupon working electrode (iron, copper, or stainless steel), A saturated Ag/AgCl reference electrode, and A platinum foil counter electrode. Tafel polarization curves were acquired for each DES-metal combination using a CHI760E electrochemical workstation. Meanwhile, thanks to the special analysis in the CHI760E software for the Tafel curves to calculate the corrosion current. Then, corrosion current density can be obtained from Equation (1), and the corrosion rate can be calculated by Equation (2).[28]

$$I_{corr} = \frac{i}{A} \quad (1)$$

$$CR = \frac{3.28 \times I_{corr} \times M}{\rho n} \quad (2)$$

Where I_{corr} (mA/cm^2) and i (mA) are the corrosion current density and the current density, respectively. A (cm^2), ρ (g/cm^3), and M (g/mol) are the area, density, and molecular weight of metal, respectively. CR (mm/year) and n are the corrosion rate of DESs to metals and the number of electrons involved in the redox reaction, respectively.

Vapor pressure. Vapor pressure, a critical determinant of liquid desiccant dehumidification efficiency, was predicted for all DES samples using first-principles molecular modelling. The 3D chemical structures of L-Arginine, L-Proline, and Glycerol were retrieved from the PubChem database and were shown in Figure S2. Their geometry structures were optimized using Materials Studio 2019 (BIOVIA) and corresponding COSMO files for each Hydrogen Bond Acceptor (HBA) and Hydrogen Bond Donor (HBD) component were subsequently imported into BIOVIA COSMOtherm 2021. This enabled theoretical computation of temperature-dependent vapor pressures across the evaluated DES compositions via the thermodynamic framework.

RESULTS AND DISCUSSION

Density and surface tension

As illustrated in Figure 2, the densities of all samples decreased with increasing temperature. This phenomenon can be attributed to the rise in molecular kinetic energy at higher temperatures, which facilitates the ability of molecules to overcome the intermolecular forces, thereby increasing their free volume. Additionally, the density of the samples decreased as the ratio of hydrogen bond donors (HBD) increased. This effect is likely due to the limited number of hydrogen bond acceptor (HBA) sites available; when the proportion of HBD exceeds the capacity of HBA to form hydrogen bonds, the excess HBD molecules remain unbound and occupy space in a free state, resulting in an increased volume for a given mass of deep eutectic solvents (DESs). Furthermore, the reduction in density was more pronounced with increasing water content compared to increasing glycerol content. This can be explained by two factors: firstly, the increment in water content was greater than that of glycerol in each experimental step; secondly, due to the limited hydrogen bond acceptor sites of HBA, most of the added water remained unbound, and since water has a relatively low density, its presence further contributed to the overall decrease in density.

Figure 3 demonstrates that the surface tension of deep eutectic solvents (DESs) decreases with increasing temperature. This trend can be attributed to the fact that elevated temperatures increase the average distance between molecules, thereby weakening intermolecular attractions and reducing the cohesive forces acting on molecules at the surface layer. Furthermore, the surface tension of the AG series was consistently higher than that of the PG series. This observation can be explained by the greater number of hydrogen bond donors and acceptors present in L-Arginine compared to L-Proline, resulting in a higher density of hydrogen bonds per unit volume in the AG series. Consequently, the intermolecular forces in the AG series are significantly enhanced, leading to increased surface tension.

Additionally, the differences in the number of hydrogen bond donors and acceptors among L-Arginine, glycerol, and L-Proline contribute to the distinct trends observed in the surface tension of the AG and PG series as the glycerol ratio increases. Specifically, glycerol possesses fewer hydrogen bond donors and acceptors than L-Arginine but more than L-Proline. As the proportion of glycerol increases, the relative amounts of both L-Arginine and L-Proline decrease. This results in a reduction in the total number of hydrogen bonds in the AG series, whereas the total number of hydrogen bonds in the PG series increases. Therefore, with increasing glycerol content, the surface tension of the AG series decreases, while that of the PG series increases.

As the water content increased, the relative proportions of L-Arginine, L-Proline, and glycerol in the mixtures decreased correspondingly. In the AG

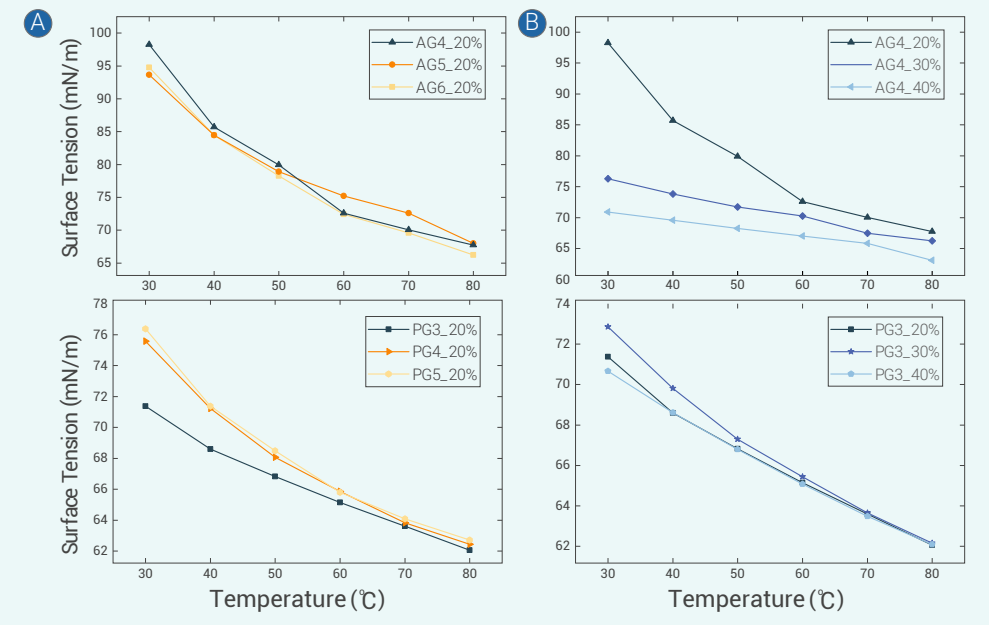

Figure 3. Surface tensions of DESs

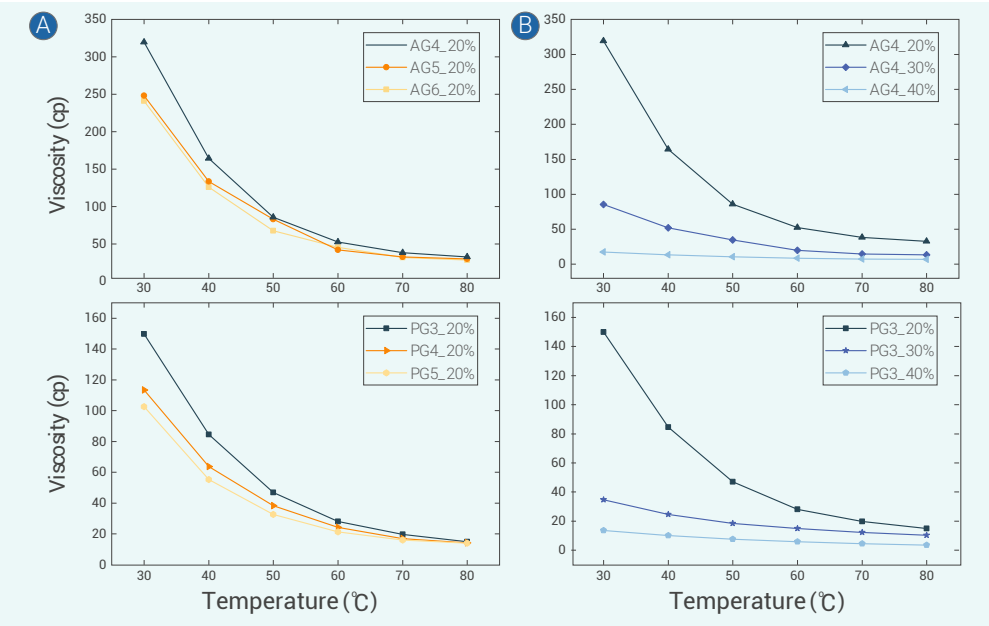

Figure 4. Viscosities of DESs

series, which initially possessed a high density of hydrogen bonds, the reduction in the concentrations of L-Arginine and glycerol led to a rapid decline in hydrogen bond formation, resulting in a pronounced decrease in surface tension. In contrast, the PG series contained comparatively fewer hydrogen bonds. When the water content increased from 20% to 30%, the reduction in hydrogen bonding was counterbalanced by the addition of water, which possesses inherently high surface tension, thereby causing an overall increase in the surface tension of the mixture. However, with further increases in water content, the overall hydrogen bond density in the DESs became extremely low, leading to a rapid decrease in surface tension.

Viscosity

Figure 4 indicates that the viscosity of the AG series is higher than that of the PG series. This can be attributed to the greater number of hydrogen bonds present in the AG series, which results in stronger intermolecular forces and, consequently, greater resistance to flow. The observed decrease in viscosity with increasing glycerol ratio, water content, and temperature can be effectively explained by the Hole Theory. According to this theory, the movement of large molecules, such as those in the AG and PG series, is hindered by the limited size of available free volume, or "holes," within the liquid matrix. The radius of these holes is directly proportional to temperature and inversely proportional to the surface tension of the components. Therefore, as the proportion of low-surface-tension components such as glycerol and water increases and as temperature rises, the radius of the holes within the DESs expands, facilitating molecular movement and thereby reducing viscosity.

Moreover, an increase in water content has a more pronounced effect on reducing the viscosity of DESs compared to an increase in the glycerol ratio. This is primarily because the addition of water significantly disrupts the hydrogen bonding network, substantially weakening intermolecular interactions and leading to a marked decrease in viscosity.

Vapor pressure

Wu et al.[52] designed various types of deep eutectic solvents (DESs) and experimentally measured their vapor pressures using the static method. The experimental vapor pressure data for ethaline (a mixture of choline chloride

and ethylene glycol) were subsequently employed to validate the accuracy of vapor pressure predictions obtained using the COSMOtherm software. The specific parameters of ethaline utilized for this validation are summarized in table (see Figure 5). Figure 5 shows that comparison between experimental and theoretical results of vapor pressure; the maximum relative error between those two was less than 16%. That proves the reliability of theoretical results.

As shown in Figure 6, the vapor pressure of the DESs decreased with increasing glycerol ratio. In the AG series, although an increase in the glycerol ratio reduced the total number of hydrogen bonds—an effect that would typically increase vapor pressure—the accumulation of low-volatility glycerol at the surface of the DESs led to a substantial decrease in vapor pressure. The higher the glycerol ratio, the more pronounced this decrease, effectively offsetting the impact of reduced hydrogen bonding. Similarly, in the PG series, increasing the glycerol ratio resulted in a greater total number of hydrogen bonds, which, together with the surface accumulation of glycerol, further suppressed vapor pressure. Consequently, the reduction in vapor pressure observed in the PG series was even more significant than that in the AG series, due to the combined effects of enhanced hydrogen bonding and surface glycerol enrichment.

In contrast, as the water content increased, both the number of hydrogen bonds and the glycerol ratio in the DESs declined rapidly, leading to a sharp increase in vapor pressure. Under these conditions, the vapor pressure of the DESs approached that of pure water. This can be attributed to the disruption of the DES hydrogen bond network by excess water, as well as the increased presence of free water molecules. As a result, the hygroscopicity of the DESs and their capacity to retain absorbed moisture were significantly diminished.

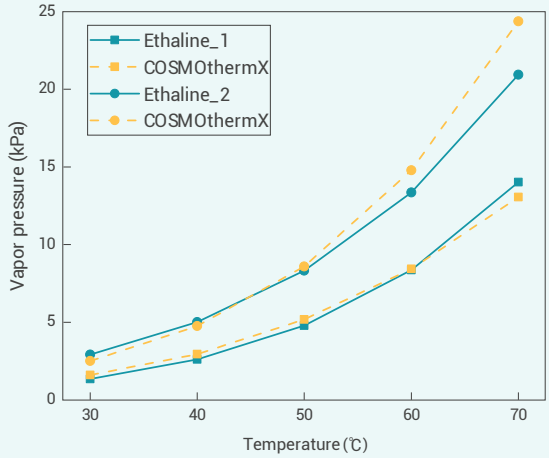

Ethaline	Choline Chloride	Ethylene Glycol	Water
1	1 mol	2 mol	0.60988 mol
2	1 mol	2 mol	1.62675 mol

Figure 5. Comparison of predicted and experimental vapor pressure

Tafel curve and corrosion rate

Figure 7 presents the Tafel curves for various metals, using AG4_20% and PG3_20% as representative examples. The corresponding corrosion rates of different solutions on these metals are detailed in the image on the right. Notably, the majority of DESs exhibited lower corrosion rates on metals compared to water. This can be attributed to the extensive hydrogen bond network within DESs, which restricts the mobility of metal ions. Additionally, water molecules—an essential medium for facilitating electrochemical corrosion—are similarly constrained by the hydrogen bond network when incorporated into DESs, thereby reducing their activity and, consequently, the corrosion rate. The PG series demonstrated superior corrosion resistance relative to the AG series. In the PG series, the lower density of hydrogen bonds allows a greater proportion of glycerol molecules to diffuse freely to the metal surface, where they can adsorb via hydroxyl groups and form a protective layer. This layer serves as a physical barrier, isolating the metal from the corrosive environment, and can also establish a hydrophobic interface that repels water. Furthermore, the presence of three hydroxyl groups in glycerol enables more extensive surface coverage, thereby inhibiting the initiation and propagation of pitting corrosion. The methodology for calculating corrosion rates is illustrated using tap water as an example, with specific calculation parameters provided in table (see Figure 7). According to the study by Feng et al.,[53] the corrosion current density of tap water on copper was 2.10×10^{-3} mA/cm^2. The relative error between the results obtained in this work and those reported in the reference was 1.14%.

DESs vs. LiBr solution

As potential alternatives to conventional dehumidification solutions, the thermal properties of deep eutectic solvents (DESs) are summarized in table (see Figure 8) and Figure 8 and compared with those of lithium bromide (LiBr) solution. The most significant distinction between the thermal properties of DESs and LiBr solution lies in their viscosities. DESs exhibit substantially higher viscosities than LiBr solution, primarily due to the strong intermolecular forces arising from extensive hydrogen bonding within DESs. These hydrogen bonds contribute to greater resistance to flow, resulting in higher viscosity compared to the predominantly ionic interactions present in LiBr solution.

Theoretical results indicate that the vapor pressure of DESs is higher than that of LiBr solution. This can be attributed to the disruption of the hydrogen bond network in DESs by excessive water content, which diminishes their capacity to retain water molecules. In contrast, the primary intermolecular forces in halide solutions such as LiBr are ion-dipole interactions, which enable the solution to strongly adsorb and immobilize water molecules. As a result, it becomes significantly more difficult for water molecules to overcome these forces and transition into the gas phase, leading to a markedly lower vapor pressure for LiBr solutions. Furthermore, the vapor pressure of DESs can be effectively reduced by decreasing the water content. For example, when the water content was reduced by 15% compared to DESs containing 20% water, the vapor pressure decreased by as much as 61%.

As illustrated in Figure 8, DESs exhibit lower corrosion rates on metals compared to LiBr solution. Both the hydrogen bond network in DESs and the ion-dipole interactions in LiBr solution facilitate the adsorption of water molecules. However, halide ions in LiBr possess strong penetrating and disruptive effects on the passivation films that naturally form on metal surfaces. This disruption exposes the underlying metal directly to the solution, rendering it susceptible to anodic electrochemical corrosion and thereby significantly accelerating the corrosion rate. In contrast, the hydrogen bond network in DESs restricts the mobility of water molecules, and the presence of free hydrogen bond acceptors (HBA) and donors (HBD) does not compromise the integrity of the metal passivation film. As a result, DESs can reduce metal corrosion rates to as low as 0.001 mm/year.

Design strategy of new DESs

Three key properties critically influence the dehumidification performance of liquid desiccants: vapor pressure, corrosion rate toward metals, and viscosity. Vapor pressure determines the hygroscopic capacity and operational limit of liquid desiccants. Corrosion rate significantly impacts the service life and maintenance costs of liquid desiccant air conditioning systems (LDAS). Excessive viscosity not only leads to carryover issues but also increases the energy consumption required for pumping and circulation. Theoretical calculations indicate that reducing the water content is the most effective approach to lowering the vapor pressure of DESs. However, it should be noted that the viscosities of DESs are substantially higher than those of halide solutions. Experimental results further demonstrate that increasing the water content markedly decreases the viscosity of DESs. Nevertheless, excessive water content results in elevated vapor pressure, thereby diminishing the dehumidification capacity of DESs. Therefore, the optimal design strategy for new DESs involves selecting hydrogen bond donors (HBDs) with inherently low viscosity, such as ethylene glycol, and minimizing the water content to a range of approximately 4%–10%. This approach aims to achieve a balance between low vapor pressure and manageable viscosity, thereby enhancing the overall dehumidification perfor-

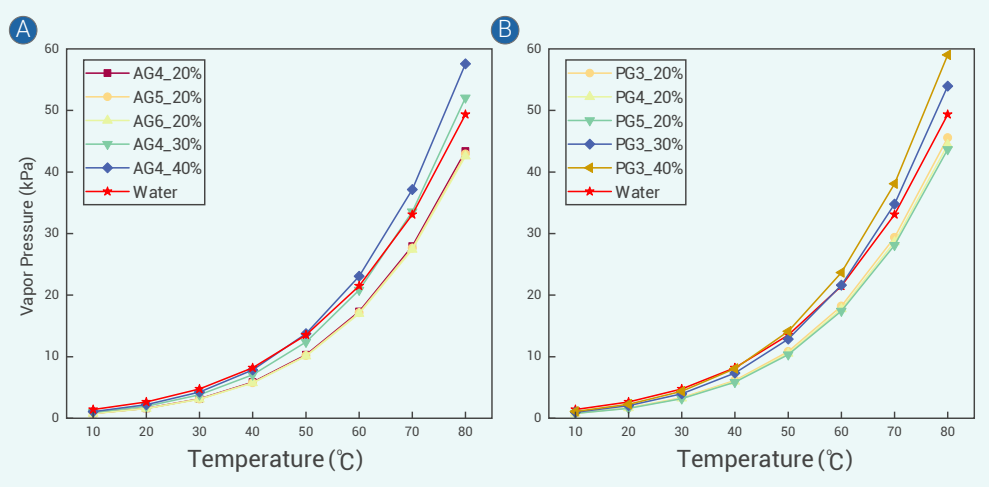

Figure 6. Vapor pressure of DESs at various temperatures

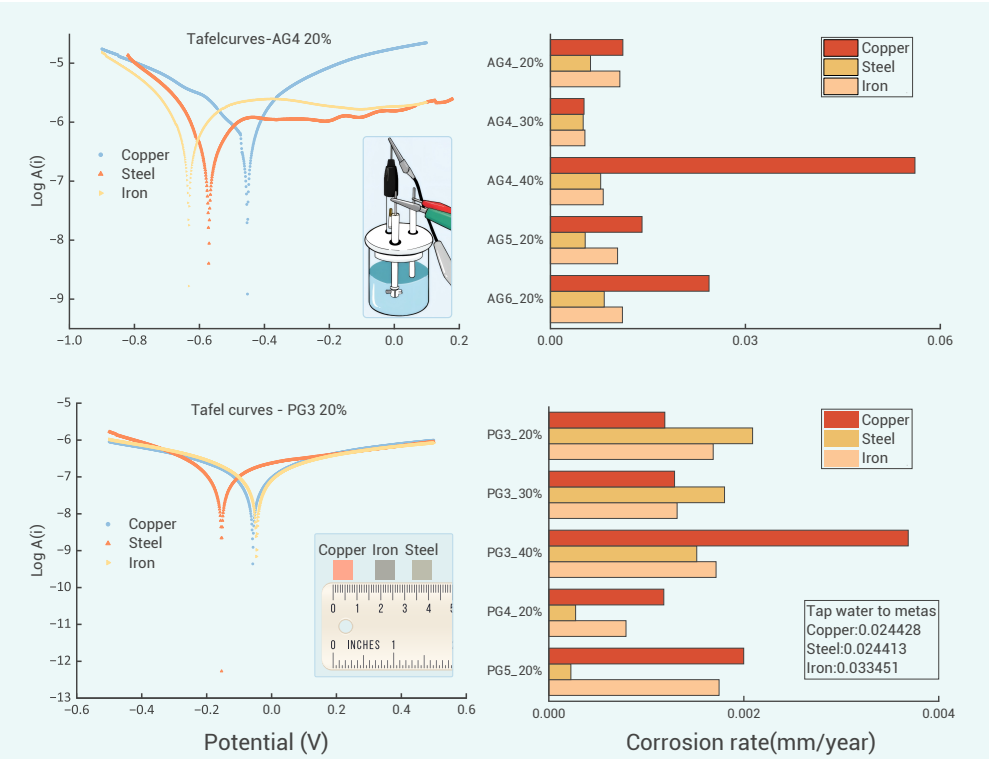

Solution	Metal	Icorr (mA/cm2)	M (g/mol)	ρ (g/cm^3)	n	Corrosion rate
Tap water	Iron	2.86E-03	56	7.86	2	0.03345099
	Steel	2.10E-03	56	7.9	2	0.02441317
	Copper	2.08E-03	64	8.92	2	0.02442791

Figure 7. Tafel Curves and corrosion rates of DESs to various metals

mance of DESs.

CONCLUSIONS

Liquid desiccant is a key component of an LDAS that affects the system's dehumidification efficiency, cost, and design selection. Conventional liquid desiccants such as LiCl, LiBr, and $CaCl_2$ solutions with high corrosivity to metals affect the lifetime and material selection of the whole system. Researchers proposed weak organic acid salts and ILs with a lower corrosion rate to metals that have the potential to replace the conventional liquid desiccants. However, the weak moisture removal capacity of weak acid salt solution, and the high cost and viscosity of ILs limited their application in LDAS. DESs have attracted increasing attention in LDAS applications due to their characteristics of being non-corrosive, non-volatile, and non-toxic. A novel DES based on amino acids as HBA was proposed in this work. The effects of HBA type, HBD ratio, and water content on its physicochemical properties were investigated using experimental and theoretical methods.

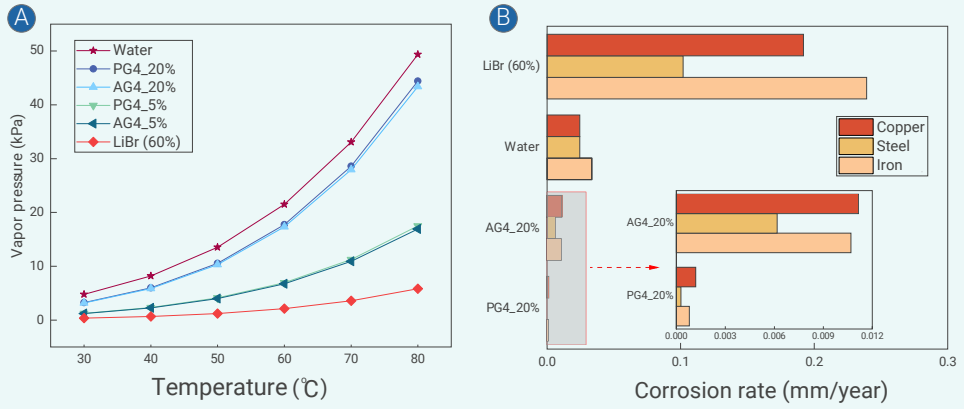

Solution	Density ρ (g/cm^3)	Viscosity (cp)	Surface tension (mN/m)
LiBr(60%)	1.723	7.73	93.51
AG4_20%	1.226	319.5	98.26
PG4_20%	1.222	113.4	75.58

Figure 8. Comparisons of vapor pressure and corrosion rate

The main conclusions were as follows.

(1) The densities, surface tensions, and viscosities of the DESs decreased with increasing temperature, HBD ratio, and water content, except for the surface tension in the PG series. There was minimal difference in density and surface tension between the AG and PG series. Additionally, DESs utilizing L-Proline as the HBA exhibited lower viscosities than those with L-Arginine as the HBA.

(2) The vapor pressure of the novel DESs containing 20% water was slightly lower than that of pure water. Vapor pressure decreased with increasing HBD ratio and increased with higher water content. Theoretical calculations further indicated that the vapor pressure of DESs can be significantly reduced by lowering the water content.

(3) Comparative experimental results on the corrosivity toward copper, stainless steel, and iron demonstrated that the PG series exhibited the lowest corrosion rates among all tested solutions, including 60% LiBr solution, tap water, and the AG series. Given their low corrosion rates, as well as favourable vapor pressure and viscosity profiles, DESs show considerable potential as replacements for halide solutions in LDAS applications.

(4) The optimal design strategy for developing DESs suitable for LDAS applications involves selecting hydrogen bond donors (HBDs) with inherently low viscosity and minimizing the water content in the DES formulation.

REFERENCES

1. Zhang Y., Zhang H., Yang H., et al. (2023). Optimization of the Liquid Desiccant Cooling Systems in Hot and Humid Areas. *Sustainability* **15**:13511. DOI:10.3390/su151813511
2. Bai Z., Chinnappan A., Deng J., et al. (2023). Recent progress in ionic liquids as desiccants for energy consumption in cooling applications. *J. Mole. Liquid.* **383**:122033. DOI:10.1016/j.molliq.2023.122033
3. Zhang Y., Zhang H., Yang H., et al. (2023). Response surface modeling and optimization scheme of an internally cooled liquid desiccant air conditioning system. *J. Build. Eng.* **76**:107371. DOI:10.1016/j.jobe.2023.107371
4. Yamaguchi S., Matsushita S., Jeong J., et al. (2006). Characteristics evaluation of absorption type dehumidifier using aqueous LiCl solution. *Proceed. 3rd ACFA.* **1**:345.
5. Lazzarin R.M., Gasparella A. and Longo G.A. (1999). Chemical dehumidification by liquid desiccants: theory and experiment. *I. J. Refrig.* **22**:334-47. DOI:10.1016/S0140-7007(98)00044-9
6. Kinsara A.A., Elsayed M.M. and AlRabghi O.M. (1996). Proposed energy-efficient air-conditioning system using liquid desiccant. *Appl. Therm. Eng.* **16**:791-806. DOI:10.1016/1359-4311(95)00090-9
7. Gurubalan A., Maiya M.P. and Geoghegan P.J. (2019). A comprehensive review of liquid desiccant air conditioning system. *Appl. Energy* **254**:113673. DOI:10.1016/j.apenergy.2019.113673
8. Rafique M.M., Gandhidasan P. and Bahaidarah H.M.S. (2016). Liquid desiccant materials and dehumidifiers - A review. *Renew. Sustain. Energy Rev.* **56**:179-95. DOI:10.1016/j.rser.2015.11.061
9. Wen T., Lu L., Nie Y.D., et al. (2019). Development and investigation on the dehumidification and corrosion resistance performance of a new mixed liquid desiccant. *I. J. Heat Mass Trans.* **130**:72-82. DOI:10.1016/j.ijheatmasstransfer.2018.10.066
10. Fekadu G. and Subudhi S. (2018). Renewable energy for liquid desiccants air conditioning system: A review. *Renew. Sustain. Energy Rev.* **93**:364-79. DOI:10.1016/j.rser.2018.05.016
11. Luo J. and Yang H. (2022). A state-of-the-art review on the liquid properties regarding energy and environmental performance in liquid desiccant air-conditioning systems. *Appl. Energy* **325**:119853. DOI:10.1016/j.apenergy.2022.119853
12. Tsai E.S., Jiang H. and Panagiotopoulos A.Z.(2016). Monte Carlo simulations of H2O-CaCl2 and H2O-CaCl2-CO2 mixtures. *Fluid Phase Equil.* **407**:262-8. DOI:10.1016/j.fluid.2015.05.036
13. Peters R. and Keller J.U. (1994). Solvation model for VLE in the system H2O-LiBr from 5 to 76 wt%. *Fluid Phase Equilibria.* **94**:129-47. DOI:10.1016/0378-3812(94)87054-3
14. Pátek J. and Klomfar J. (2008). Thermodynamic properties of the LiCl-H2O system at vapor-liquid equilibrium from 273 K to 400 K. *I. J. Refrig.* **31**:287-303. DOI:10.1016/j.ijrefrig.2007.05.003
15. Okada K., Nakanome M., Kameshima Y., et al. (2010). Water vapor adsorption of CaCl2-impregnated activated carbon. *Mater. Res. Bullet.* **45**:1549-53. DOI:10.1016/j.materresbull.2010.07.027
16. Ye H., Yuan Z., Li S.M., et al. (2014). Activated carbon fiber cloth and CaCl2 composite sorbents for a water vapor sorption cooling system. *Appl. Therm. Eng.* **62**:690-6. DOI:10.1016/j.applthermaleng.2013.10.035
17. Wang J., Wang R. and Wang L. (2016). Water vapor sorption performance of ACF-CaCl2 and silica gel-CaCl2 composite adsorbents. *Appl. Therm. Engi.* **100**:893-901. DOI:10.1016/j.applthermaleng.2016.02.100
18. Yao Y., Yu Y. and Zhu Z. (2016). Experimental investigations on surface vapor pressure models for LiCl-CaCl2 desiccant solutions. *Solar Energy* **126**:1-13. DOI:10.1016/j.solener.2015.12.046
19. Kol S. and Arya M. (2025). Performance optimization of a baffle plate falling film dehumidifier using nanocarbon tube-enhanced LiCl/H_2O solution. *I. Commun. Heat Mass Trans.* **167**:109296. DOI:10.1016/j.icheatmasstransfer.2025.109296
20. Tsai C.Y., Soriano A.N. and Li M. (2009). Vapour pressures, densities, and viscosities of the aqueous solutions containing (triethylene glycol or propylene glycol) and (LiCl or LiBr). *J. Chem. Therm.* **41**:623-31. DOI:10.1016/j.jct.2008.12.022
21. Królikowska M., Romanska K., Paduszynski K., et al. (2020). The study on the influence of glycols on the vapor pressure, density and dynamic viscosity of lithium bromide aqueous solution. *Fluid Phase Equil.* **519**:112640. DOI:10.1016/j.fluid.2020.112640
22. Leiva-García R., Muñoz-Portero M.J., García-Antón J., et al. (2012). Effects of Hydrodynamic Conditions and LiBr Concentration on the Corrosion of Copper in LiBr

Absorption Machines. *I. J. Electrochem. Sci.* **7**:1332-47. DOI:10.1016/S1452-3981(23)13417-1
23. Kiey S.A.A., Meguid E.A.A. and Rehim S.S.A. (2023). Electrochemical Investigations on the Corrosion Behavior of 904L Stainless Steel in LiBr Solutions. *J. Mater. Eng. Perform.* **32**:9163-73. DOI:10.1007/s11665-023-08080-4
24. Li J., Liang C., Huang N., et al. (2012). Corrosion of steel in lithium bromide solution containing inhibitor. *Corros. Eng. Sci. Techn.* **47**:297-301. DOI:10.1179/1743278212Y.0000000011
25. Larios-Galvez A.K., Lopez-Sesenes R., Sarmiento-Bustos E., et al. (2022). Corrosion Behavior of Steels in LiBr-H2O-CaCl2-LiNO3 Systems. *Metals* **12**. DOI:10.3390/met12020279
26. Park T.J. and Jang H. (2021). Effects of Inhibitors on Corrosion Resistance of Steel in CaCl2 Solution Based on Response Surface Analysis. *Corros. Sci. Techn. Korea* **20**:129-42. DOI:10.14773/cst.2021.20.3.129
27. Avilés-Flores M., Larios-Gálvez A.K., Martínez-González J., et al. (2024). Corrosion Behavior of Carbon Steel in LiCl/H2O Mixtures. *Metals* **14**. DOI:10.3390/met14040376
28. Wen T., Lu L., Li M., et al. (2018). Comparative study of the regeneration characteristics of LiCl and a new mixed liquid desiccant solution. *Energy* **163**:992-1005. DOI:10.1016/j.energy.2018.08.188
29. Giampieri A., Ma Z., Smallbone A., et al. (2018). Thermodynamics and economics of liquid desiccants for heating, ventilation and air-conditioning - An overview. *Appl. Energy* **220**:455-79. DOI:10.1016/j.apenergy.2018.03.112
30. Wen T., Wang M., Chen Y., et al. (2019). Thermal properties study and performance investigation of potassium formate solution in a falling film dehumidifier/regenerator. *I. J. Heat Mass Trans.* **134**:131-42. DOI:10.1016/j.ijheatmasstransfer.2019.01.031
31. Wen T., Luo Y. and Sheng L. (2020). Experimental study on the corrosion behavior and regeneration performance of KCOOH aqueous solution. *Solar Energy* **201**:638-48. DOI:10.1016/j.solener.2020.03.044
32. Wen T., Luo Y., Wang M., et al. (2020). Comparative study on the liquid desiccant dehumidification performance of lithium chloride and potassium formate. *Renew. Energy* **167**:841-52. DOI:10.1016/j.renene.2020.11.157
33. Rippy K.C., Volk E., Beers R., et al. (2022). Corrosion of Metal Alloys in Potassium Acetate Solutions for Liquid Desiccant Dehumidification and Air Conditioning. *Energies* **15**. DOI:10.3390/en15124421
34. Salikandi M., Ranjbar B., Shirkhan E., et al. (2020). Thirunavukkarasu I, Sudhakar K. Recent trends in liquid desiccant materials and cooling systems: Application, performance and regeneration characteristics. *J. Build. Eng.* **33**:101579. DOI:10.1016/j.jobe.2020.101579
35. Lee W.C., Hong Z., Chen Y., et al. (2024). Novel DABCO-Derived Ionic Liquids for Liquid Desiccant Air Conditioning. *ACS Sustain. Chem. Eng.* **12**:16249-59. DOI:10.1021/acssuschemeng.4c05343
36. Spiess A., Brandt P., Schmitz A., et al. (2021). Water sorption by ionic liquids: Evidence of a diffusion-controlled sorption process derived from the case study of [BMIm][OAc]. *J. Mole. Liquids* **348**:118023. DOI:10.1016/j.molliq.2021.118023
37. Maekawa S., Matsumoto R., Ito K., et al. (2020). Design of quaternary ammonium type-ionic liquids as desiccants for an air-conditioning system. *Green Chem. Eng.* **1**:109-16. DOI:10.1016/j.gce.2020.09.016
38. Luo Y., Shao S., Qin F., et al. (2012). Investigation on feasibility of ionic liquids used in solar liquid desiccant air conditioning system. *Solar Energy.* **86**:2718-24. DOI:10.1016/j.solener.2012.06.008
39. Qu M., Abdelaziz O., Sun X., et al. (2017). Aqueous solution of [EMIM][OAc]: Property formulations for use in air conditioning equipment design. *Appl. Therm. Eng.* **124**:271-8. DOI:10.1016/j.applthermaleng.2017.05.167
40. Wang L., Liu X., Qu M., et al., (2022). Bahar B. An experimental study on dehumidification and regeneration performance of a new nonporous membrane-based heat and mass exchanger using an ionic liquid desiccant. *Energy Build.* **254**:111592. DOI:10.1016/j.enbuild.2021.111592
41. Watanabe H., Komura T., Matsumoto R., et al. (2019). Design of ionic liquids as liquid desiccant for an air conditioning system. *Green Energy Environ.* **4**:139-45. DOI:10.1016/j.gee.2018.12.005
42. Cao B., Yin Y., Kim M., et al. (2024). Characteristics of heat and mass transfer in moist air-ionic liquid desiccant bubbly systems: Parametric assessment of regeneration performance. *Appl. Therm. Eng.* **257**:124487. DOI:10.1016/j.applthermaleng.2024.124487
43. Cao B., Yin Y., Xu G., et al. (2023). A proposed method of bubble absorption-based deep dehumidification using the ionic liquid for low-humidity industrial environments with experimental performance. *Appl. Energy* **348**:121534. DOI:10.1016/j.apenergy.2023.121534
44. Cao B., Yin Y., Xu G., et al. (2023). Experimental and modeling study of bubble absorption-based deep dehumidification using the ionic liquid: Parametric analysis on heat and mass transfer. *Energy Conver. Manag.* **290**:117169. DOI:10.1016/j.enconman.2023.117169
45. Cao B., Yin Y., Zhang F., et al. (2023). Liquid desiccant-based deep dehumidifier working with a novel ionic liquid: Prediction model and performance comparison. *I. J. Refrig.* **146**:74-87. DOI:10.1016/j.ijrefrig.2022.09.033
46. Oladosu T.L., Baheta A.T. and Oumer A.N. (2021). Desiccant solutions, membrane technologies, and regeneration techniques in liquid desiccant air conditioning system. *I. J. Energy Res.* **45**:8420-47. DOI:10.1002/er.6482
47. Oladosu T.L., Al-Kayiem H.H., Gilani S.I.U., et al. (2021). Dehumidification and thermal regeneration characterization of binary deep eutectic solvents in liquid desiccant air conditioning systems. *J. Build. Eng.* **42**:103056. DOI:10.1016/j.jobe.2021.103056
48. Oladosu T.L., Pasupuleti J., Tiong S.K., et al. (2025). Magnetic field-enhanced electrodialysis regeneration of deep eutectic solvent as a greener desiccant for air dehumidification. *J. Build. Eng.* **104**:112318. DOI:10.1016/j.jobe.2025.112318
49. Oladosu T.L., Al-Kayiem H.H., Gilani S.I.H., et al. (2023). Performance enhancement of electrodialysis regeneration of deep eutectic solvent for liquid desiccant air conditioning systems. *J. Build. Eng.* **70**:106343. DOI:10.1016/j.jobe.2023.106343
50. Luo J. and Yang H. (2023). Energy, exergy, exergoeconomic and enviroeconomic (4E) assessment on a liquid desiccant air-conditioning system using green deep eutectic solvent of ethaline. *Energy Conver. Manag.* **277**:116685. DOI:10.1016/j.enconman.2023.116685
51. Zhang Y., Chen Y., Luo J., et al. (2025). Improving air conditioning efficiency using solar-assisted liquid desiccant systems: Experimental and simulation analysis of two desiccants. *Renew. Energy* **253**:123572. DOI:10.1016/j.renene.2025.123572
52. Wu S., Caparanga A.R., Leron R.B., et al. (2012). Vapor pressure of aqueous choline chloride-based deep eutectic solvents (ethaline, glyceline, maline and reline) at 30-70 °C. *ThermoChim. ACTA.* **544**:1-5. DOI:10.1016/j.tca.2012.05.031
53. Feng Y., Teo W.K., Siow K.S., et al. (1996). The corrosion behaviour of copper in neutral tap water. 2. Determination of corrosion rates. *Corros. Sci.* **38**:387-95. DOI:10.1016/0010-938X(96)00111-4

FUNDING AND ACKNOWLEDGMENTS

The work described in this paper was supported by grants from the General Research Fund project of the Hong Kong Research Grant Council (Ref. No.: 15208024).

AUTHOR CONTRIBUTIONS

All authors contributed to the manuscript and approved the final version.

DECLARATION OF INTERESTS

The authors declare no competing interests.

DATA AND CODE AVAILABILITY

Data are available from the corresponding author upon reasonable request.

SUPPLEMENTAL INFORMATION

Supplementary materials are available at: https://doi.org/10.59717/ipj.energy-use.2025.100004